Fermi surface nesting and charge-density wave formation in rare-earth tritellurides

J. Laverock, S. B. Dugdale, Zs. Major, and M. A. Alam

H. H. Wills Physics Laboratory, University of Bristol,
Tyndall Avenue, Bristol BS8 1TL, United Kingdom

N. Ru and I. R. Fisher

Geballe Laboratory for Advanced Materials and Department of Applied Physics,
Stanford University, Stanford, California 94305-4045

G. Santi

Department of Physics and Astronomy, University of Aarhus, DK-8000 Aarhus C, Denmark

E. Bruno

Department of Physics, University of Messina, Salita Sperone 31, 98166 Messina, Italy
(Dated: February 2, 2008)

The Fermi surface of rare-earth tri-tellurides (RTe$_3$) is investigated in terms of the nesting driven charge-density wave formation using positron annihilation and first-principles LMTO calculations. Fermi surface nesting is revealed as a strong candidate for driving charge-density wave formation in these compounds. The nesting vector obtained from positron annihilation experiments on GdTe$_3$ is determined to be $\mathbf{q} = (0.28 \pm 0.02, 0, 0)\,\mathbf{a}^*$, $(\mathbf{a}^* = 2\pi/\mathbf{a})$, in excellent agreement with previous experimental and theoretical studies.

I. INTRODUCTION

The existence of charge-density wave (CDW) ground states in low dimensional metals has attracted a great deal of interest over many years (see for example [1, 2, 3]). It is well known that instabilities in the Fermi surface (FS) due to particular features of the electronic band structure (e.g. nesting features, van Hove saddle points) can lead to the emergence of new ground states such as spin-density [4] or charge-density waves [5]. Examples of systems where this is thought to be the case include the transition metal dichalcogenides [1], pure Cr [4] and organic charge-transfer salts [2]. While the underlying electronic band structure of a system whose new periodicity is commensurate with the lattice is well understood, the behavior in cases where the periodicities are incommensurate is much less clear [6].

Motivated by recent angle-resolved photoemission (ARPES) studies aimed at clarifying this issue [7, 8], we have combined first-principles electronic structure calculations and positron annihilation experiments to establish the FS topologies of a model CDW system, namely the rare earth tritellurides.

In systems whose FS topologies include large parallel faces spanned by a (nesting) vector $\mathbf{q}$, there will be an instability in that system towards opening up gaps on these faces by introducing some new periodicity and hence new superzone boundaries. A CDW is an example of the results of such an instability. Although in general the CDW will not be commensurate with the lattice (since its periodicity is dictated by the nesting vector), many CDWs experience "lock-in" to a suitably commensurate period, thereby lowering the strain energies associated with the distortion.

The rare-earth tritelluride series, RTe$_3$ (R = Y, La – Tm), crystallises in the layered NdTe$_3$ structure [9], and consists of sheets of inert RTe slabs sandwiched between a double-layer of square planar Te sheets (see Fig. 1). It should be noted that the crystollagraphic b-axis is the long axis. Resistivity measurements have revealed a large anisotropy (ρ_a/ρ_b) across the series, as much as ~ 5000 in the case of SmTe$_3$ [10]. The electron diffraction results of DiMasi *et al.* showed strong satellite peaks, which were interpreted as stemming from the periodic lattice distortions associated with the presence of an incommensurate CDW [11]. They report a range of wavevectors ($q \approx 0.27 - 0.31\,a^*$, $a^* = 2\pi/a$) (i.e. around $(2/7)\,a^*$) for RTe$_3$, where the CDW was found to be stable for all the rare-earths, R (from La to Tm), and occurred for most materials along both the $\mathbf{a}$ and $\mathbf{c}$ axes. In some samples, CDW formation was only observed along one of these directions, although this was found to be highly sample dependent. ARPES studies [7, 12] have successfully mapped the gap anisotropy, finding the FS to be very significantly gapped (~ 200 meV) along $\Gamma - Y$ ($\Gamma - Z$ in their coordinates); this would correspond to a temperature well beyond the samples' melting points. Further, the ARPES studies have confirmed the magnitude of the CDW wave-vector to be $q \approx (2/7)\,a^*$, equal to that observed by DiMasi *et al.* [11]. The RTe$_3$ system thus presents an unprecedented opportunity to study the correlation between the FS topology (through its nesting) and the CDW period.

The rare-earth ditellurides RTe$_2$ (Fig. 1) are a related material, crystallising in the layered tetragonal anti-Cu$_2$Sb structure [13]. In these materials, electron

diffraction reveals satellite peaks corresponding to a commensurate superstructure characterised by a $(2 \times 1 \times 1)$ supercell, attributed to CDW formation [14]. Calculations of the electronic structure of this system will be presented alongside those for $R\mathrm{Te}_3$ in order to highlight the similarities and differences.

Here we present the FS of GdTe_3 as measured by 2-dimensional angular correlation of electron-positron annihilation radiation (2D-ACAR) in conjunction with first-principles electronic structure calculations of lutetium di- and tri-tellurides.

II. ELECTRONIC STRUCTURE CALCULATIONS

The electronic band structure was calculated for both lutetium di- and tritelluride using the linearized muffin-tin orbital (LMTO) method within the atomic sphere approximation (ASA), including combined-correction terms [15]. Lu was chosen to avoid the complications associated with the description of f-electrons within the local density approximation. The parameters of the crystalline structure were 4.55Å ($b/a = 2.037$) and 4.34Å ($b/a = 5.93$) respectively, corresponding to those found for LaTe_2 in Ref. [14] and SmTe_3 in Ref. [10]. The results of the calculation were found to be relatively insensitive to changes in the lattice parameter of $\sim 5\%$, allowing us to address all the different rare-earth systems [17]. All calculations used a basis of s, p, d and f states, and self-consistency was achieved at 1568 and 1176 k-points respectively in the irreducible Brillouin zone (BZ).

Although the tritellurides are found to have very slightly orthorhombic unit cells ($a \neq c$), a square-based cell ($a = c$) is adopted (since the effects were found to be insignificant). It is worth highlighting that there will still be in-plane anisotropy in the tritellurides even for $a = c$, caused by the $R\mathrm{Te}$ layer orientation, which will be reflected in the electronic structure.

A. Lutetium ditelluride (LuTe$_2$)

The electronic band structure and FS for LuTe_2 is shown in Figs. 2 and 3 respectively. As expected, there is little electronic interaction between layers in these compounds, expressed in the small dispersion along [010] (e.g. $\Gamma - Y$ and $N - R$). We observe three bands to cross the Fermi level (E_F), principally due to $5p$ orbitals of the planar Te layer. Two of these bands result in the diamond-shaped FS, also predicted by previous calculations [14, 16, 18]. These are the sheets which show the nesting. Two further FS sheets are observed in the present calculation, forming small hole pockets centered at Y (see Fig. 3c). As may be seen in Fig. 2, the bands responsible for these two sheets only just cross E_F, and thus the presence or absence of these sheets is likely to be very sensitive to the details of the calculation (such as

the description of the Lu $4f$ electrons in the local density approximation). It is emphasised that these features are irrelevant to the nesting vector previously proposed by DiMasi $et\ al.$ [14], corresponding to a commensurate nesting vector of $q = (1/2)\ a^*$, shown in Fig. 3; our results are consistent with the existence of such a nesting vector.

B. Lutetium tritelluride (LuTe$_3$)

The LuTe_3 band structure (Fig. 4) differs most notably from LuTe_2 in the appearance of a bilayer splitting induced as a result of the coupling between the two Te planes. This is observed as a small splitting of the sheets which compose the FS (Fig. 5), and which has been reported experimentally in ARPES studies for CeTe_3 and SmTe_3 [7, 12].

Fig. 5a shows the nesting vector previously proposed for these materials, $q \sim (2/7)\ a^*$, by DiMasi $et\ al.$ [11], observed directly in ARPES studies [7, 12]. It is clear from this figure that our band structure results strongly support such potential for nesting, further emphasised by the calculation of $\chi(q)$, for $\mathbf{q}$ along [100] (see Fig. 6). This displays a clear, broad peak centered at $q \approx 0.26\ a^*$ (the width of which arises due to the splitting of the FS), corresponding to nesting between the inner and outer diamond-shaped features (as shown in Fig. 5).

Since the FS is composed of states associated with the Te layer, no appreciable difference is likely to be observed in the nesting features of $R\mathrm{Te}_3$ for different rare earth atoms, indicated by the stability of the wavevector for different R observed by DiMasi $et\ al.$ [11], and so comparisons may be made between the lutetium compounds used in the calculation and the gadolinium compounds used in the experiment (and, for that matter, the rare-earths in other studies).

III. POSITRON ANNIHILATION MEASUREMENTS OF THE FERMI SURFACE

The occupied momentum states, and hence the FS, can be accessed via the momentum distribution using the 2D-ACAR technique [19]. This well-established technique has recently been used by some of the present authors to determine the FS topology and identify nesting features in a wide range of systems [20]. A 2D-ACAR measurement yields a 2D projection (integration over one dimension) of the underlying momentum distribution. Given that the $R\mathrm{Te}_3$ series is strongly two-dimensional, the dispersion along the $\Gamma - Y$ direction is small and thus the FS is strongly two dimensional; in this case one single projection along [010] is sufficient to observe the topology of the FS. Application of the Lock-Crisp-West (LCW) prescription [21], where the $\mathbf{p}$-space momentum density is 'folded' back into the first BZ, yields a translationally invariant $\mathbf{k}$-space distribution which indicates the

level of occupancy of the states across the (projected) BZ. The FS topology expresses itself through changes in this occupancy according to whether a particular **k**-state is occupied or unoccupied for each band. The virtue of the 2D-ACAR technique in such studies is that it reveals *directly* the shape of the FS through the shape of the occupied and unoccupied regions. The effect of a charge-density wave gap on the momentum distribution will be to slightly smear the step associated with the presence of the FS; however, given that the intrinsic momentum resolution of the spectrometer is $\sim 15\%$ of the BZ, this additional smearing is negligible and hence the 2D-ACAR spectrum is insensitive to the presence of the CDW. The positron annihilation technique thus reveals the FS unreconstructed by the CDW (i.e. the ungapped FS).

The positron annihilation measurements were performed using the Bristol spectrometer. The single crystal samples were grown by slow cooling of a binary melt containing an excess of Te, as described previously by Ref. [7]. The GdTe$_3$ sample was oriented to obtain a projection along the [010] crystallographic direction, and ~ 150 million counts were accumulated at a sample temperature of ~ 80K. A maximum entropy based deconvolution routine was used to reduce the smearing caused by the finite instrument resolution [22].

The **k**-space occupation density, projected down the [010] direction, is presented in Fig. 7, alongside the occupancy obtained from the LMTO calculation. Further measurements of TbTe$_3$ were also performed at a lower statistical precision, revealing identical features to GdTe$_3$, and will not be discussed any further. Excellent agreement is observed between the experimental and theoretical BZ occupancy; the X electron pockets are clearly visible in the data, and agree in both size and shape with the theoretically determined pockets. Whereas in the ARPES studies of Ref. [12] the FS was observed to be gapped along $\Gamma - Y$ ($\Gamma - Z$ in their coordinates), in this study no such gapping is observed, the effect of the CDW being negligible when compared with the momentum resolution of the apparatus (as described above).

As the LMTO calculation highlights, the Te bands that cross the Fermi level are degenerate for the ditellurides. However, owing to coupling between the two non-equivalent square planar Te sheets in the tritellurides, these split. Whilst this splitting has been observed (for example, [7, 12]), it should be pointed out that our momentum resolution precludes observation of this small splitting of the FS in our experiment. Note, however, that the splitting, being smaller than the experimental resolution, is likely to enhance the observability of the nested Fermi surface.

The interpretation of the data in terms of nesting provides compelling evidence in support of the role of the FS in driving CDW formation. Strong nesting features, identical to those outlined in the calculated FS, are clearly visible in the data, connecting large parallel surfaces of FS (Fig. 7), and revealing a nesting vector (present in both [100] and [001] directions) connecting optimally nested portions of the experimental FS of $\mathbf{q} = (0.28 \pm 0.02, 0, 0) \, \mathbf{a}^*$. (The Fermi surface breaks have been determined from the experimental data by a "zero crossing" method [22], where the "raw" k-space occupancy map has been subtracted from the "Maximum Entropy deconvoluted" k-space occupancy of the raw data. The zero-level contour reveals the breaks due to the diamond-shaped sheets, from which the nesting vector has been extracted.) This compares favorably with the superlattice reflections observed in electron diffraction experiments [11], and with nesting vectors of $q \approx (2/7) \, a^*$ revealed via ARPES studies [7, 12].

IV. CONCLUSION

In conclusion, we have presented the experimental ungapped Fermi surface of the high-temperature CDW compound GdTe$_3$. Complementary band structure calculations on LuTe$_3$ and the related compound, LuTe$_2$, are also presented. Both the experimental and theoretical FS topologies display excellent propensity for nesting, supporting the role of the Fermi surface in driving the formation of the CDW in these compounds. The nesting features are found to be in excellent agreement with previously proposed experimental [7, 11, 12] and theoretical [11, 16, 18] studies on the RTe$_3$ series, revealing an experimental nesting vector of $\mathbf{q} = (0.28 \pm 0.02, 0, 0) \, \mathbf{a}^*$.

V. ACKNOWLEDGEMENTS

[1] J. A. Wilson, F. J. Di Salvo and S. Mahajan, Phys. Rev. Lett. **32**, 882 (1974).

[2] R. H. Friend and D. Jérome, J. Phys. C: Sol. St. Phys. **12**, 1441 (1979).

[3] J. M. Carpinelli, H. H. Weltering, E. W. .Plummer and R. Stumpf, Nature **381**, 398 (1996)

[4] A. W. Overhauser, Phys. Rev. **128**, 1437 (1962).

[5] R. L. Withers and J. A. Wilson, J. Phys. C: Sol. St. Phys. **19**, 4809 (1986).

[6] J. Voit, L. Perfetti, F. Zwick, H. Berger, G. Margariondo, G. Grüner, H. Höchst and M. Gironi, Science **290**, 501 (2001).

[7] V. Brouet, W. L. Yang, X. J. Zhou, Z. Hussain, N. Ru, K. Y. Shin, I. R. Fisher and Z. X. Shen, Phys. Rev. Lett. **93**, 126405 (2004).

[8] H. Komoda, T. Sato, S. Souma, T. Takahashi, Y. Ito and K. Suzuki, Phys. Rev. B **70** 195101 (2004).

[9] B. K. Norling and H. Steinfink, Inorg. Chem. **5**, 1488 (1966).

[10] E. DiMasi, B. Foran, M. C. Aronson and S. Lee, Chem. Mater. **6**, 1867 (1994).

[11] E. DiMasi, M. C. Aronson, J. F. Mansfield, B. Foran and S. Lee, Phys. Rev. B. **52**, 14516 (1995).

[12] G.-H. Gweon, J. D. Denlinger, J. A. Clack, J. W. Allen, C. G. Olson, E.D. DiMasi, M. C. Aronson, B. Foran and S. Lee, Phys. Rev. Lett. **81**, 886 (1998).

[13] R. Wang, H. Steinfink and W. F. Bradley, Inorg. Chem. **5**, 412 (1966).

[14] E. DiMasi, B. Foran, M. C. Aronson and S. Lee, Phys. Rev. B. **54**, 13587 (1996).

[15] B. Barbiellini, S. B. Dugdale and T. Jarlborg, Comp. Mater. Sci. **28**, 287 (2003).

[16] LSDA+U calculations have recently been used to avoid f electrons issues within the LDA. See J. H. Shim, J.-S. Kang and B. I. Min, Phys. Rev. Lett. **93** 156406 (2004).

[17] $R\mathrm{Te}_2$ crystallises in space group number 129 (P4/nmm). The internal parameters are $R(1)$: 0.25 0.25 0.2744; Te(1): 0.75 0.25 0.5; Te(2): 0.25 0.25 0.8735 (Ref. [14]). $R\mathrm{Te}_3$ crystallises in space group number 63 (Cmcm). The internal parameters are $R(1)$: 0 0.1694 0.25; Te(1): 0 0.92925 0.25; Te(2): 0 0.5706 0.25; Te(3): 0 0.2953 0.25 (Ref. [9]).

[18] A. Kikuchi, J. Phys. Soc. Jap. **67**, 1308 (1997)

[19] R. N. West, in *Proceedings of the International School of Physics << Enrico Fermi >> — Positron Spectroscopy of Solids*, edited by A. Dupasquier and A. P. Mills jr. (IOS Press, Amsterdam, 1995).

[20] See, for example S. B. Dugdale, M. A. Alam, I. Wilkinson, R. J. Hughes, I. R. Fisher, P. C. Canfield, T. Jarlborg and G. Santi, Phys. Rev. Lett. **83**, 4824 (1999) ; Zs. Major, S. B. Dugdale, R. J. Watts, G. Santi, M. A. Alam, S. M. Hayden, J. A. Duffy, J. W. Taylor, T. Jarlborg, E. Bruno, D. Benea and H. Ebert, Phys. Rev. Lett. **92**, 107003 (2004).

[21] D. G. Lock, V. H. C. Crisp and R. N. West, J. Phys. F **3**, 561 (1973).

[22] S. B. Dugdale, M. A. Alam, H. M. Fretwell, M. Biasini and D. Wilson, J. Phys.:Condens. Matt. **6**, L435 (1994).
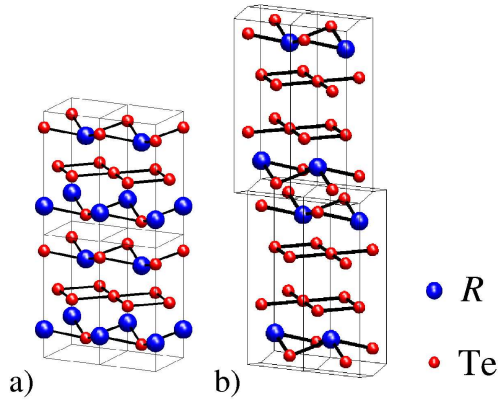
FIG. 1: (color online) The structure of (a) $R\text{Te}_2$ and (b) $R\text{Te}_3$. Note the two Te planes sandwiched between RTe layers in $R\text{Te}_3$.
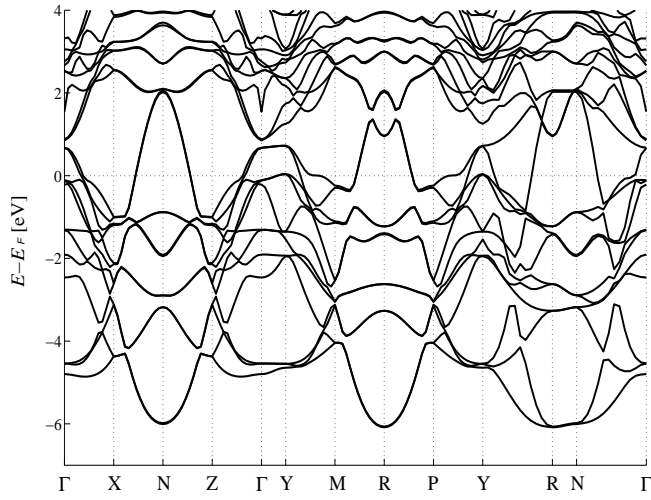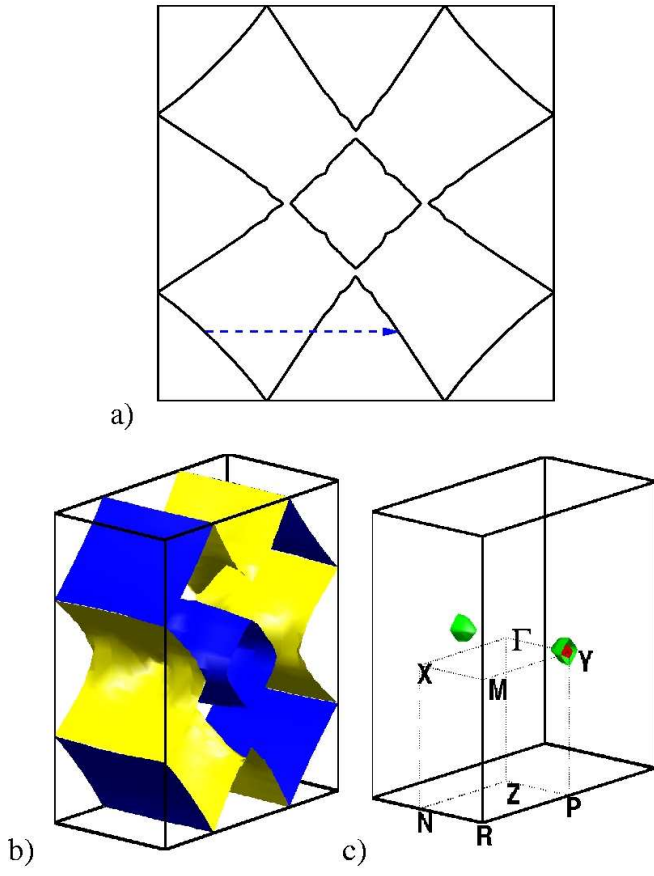

FIG. 2: The electronic band structure of LuTe$_2$.

FIG. 3: (color online) The calculated Fermi surface of LuTe$_2$ (a) on a (010) plane through Γ with the proposed nesting vector illustrated (for clarity the Y pockets have been omitted here), (b) the FS sheets responsible for the nesting, and (c) the Y-centered hole pockets. High symmetry points have been labeled in (c). The Γ-point is located at the center of the zone.
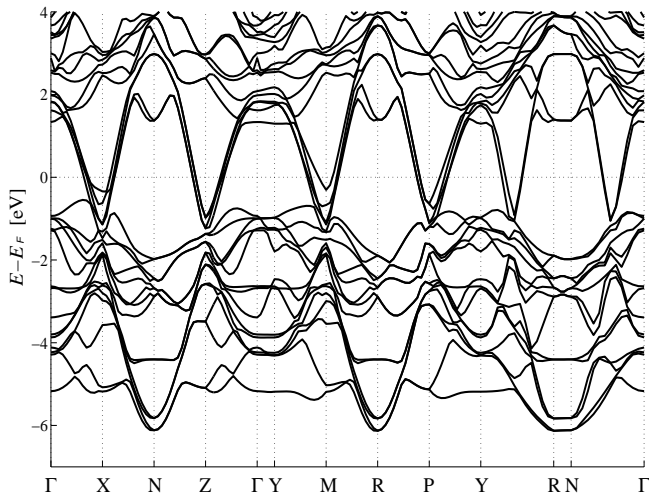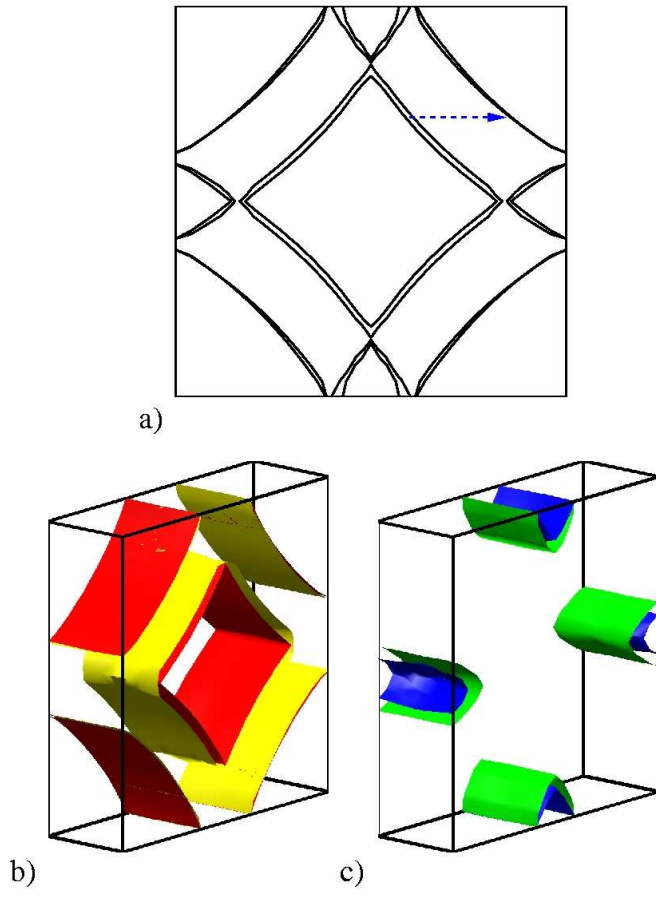

FIG. 4: The electronic band structure of LuTe$_3$.

FIG. 5: (color online) The calculated Fermi surface of LuTe$_3$ (a) on a (010) plane through Γ with the proposed nesting illustrated, (b) the two diamond shaped sheets (split by the coupling between the two Te planes) which exhibit strong nesting, and (c) the two X pockets. The symmetry points are the same as those labelled in Fig. 3.
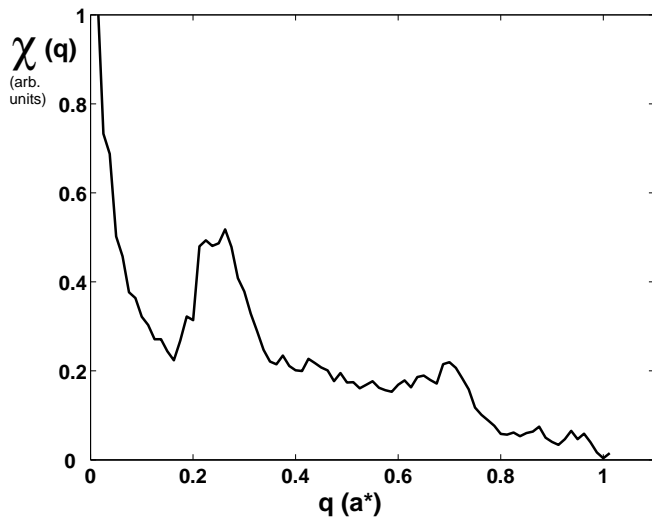
FIG. 6: The generalized susceptibility $\chi(q)$ calculated using the LMTO method for LuTe$_3$ along the [100] direction, showing the broad peak around $q \approx 0.26$ a^* due to nesting between the two diamond shaped sheets.
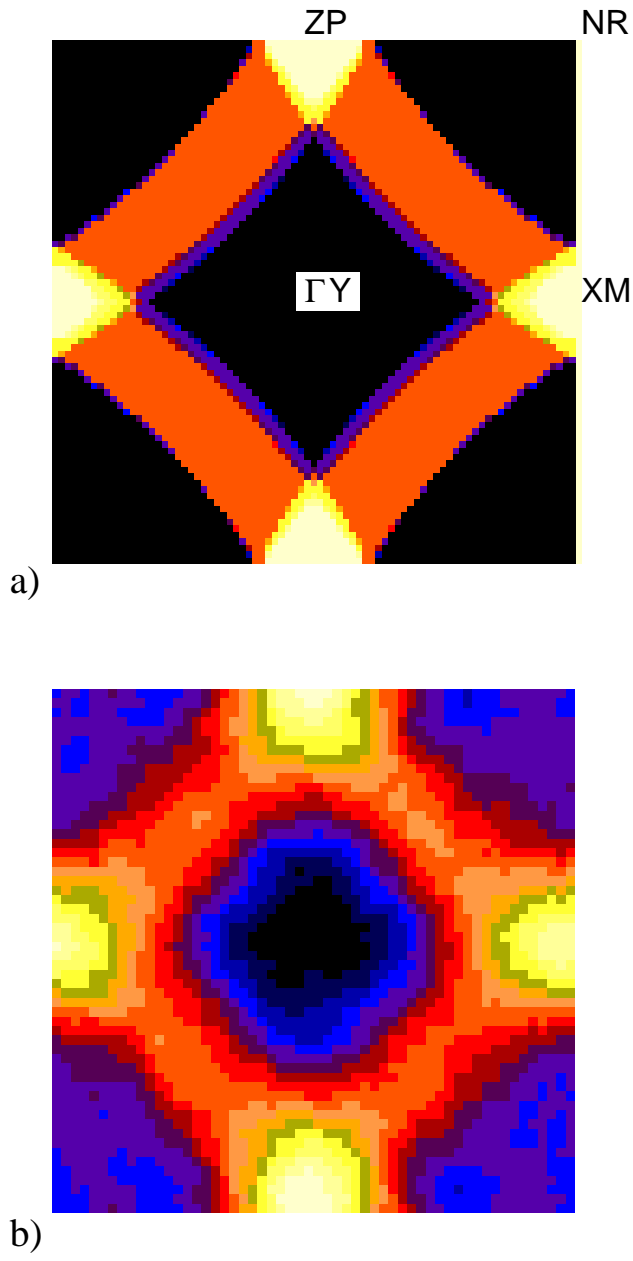
ZP   NR

ΓY   XM

a)

b)

FIG. 7: (color online) (a) Projected occupation density obtained from the LMTO calculation for LuTe$_3$, and (b) occupation density within the first BZ for GdTe$_3$ measured by the 2D-ACAR experiment. In both cases, lighter colors (shades) represent higher occupancy, and high symmetry points have been labelled in projection.